**Please cite the Published Version**

# Performance Analysis of STAR-RIS-CR-NOMA Based Consumer IoT Networks for Resilient Industry 5.0

Xingwang Li, *Senior Member, IEEE,* Xuesong Gao, Liang Yang, Hongwu Liu, *Senior Member, IEEE,* Ji Wang, *Member, IEEE,* Khaled M. Rabie, *Senior Member, IEEE,* Dawei Qiao

*Abstract*—The arrival of the sixth generation (6G) wireless communication will intensify the developments of the Internet of Things (IoT) for widely applications in resilient industry 5.0. Driving the development of the intelligent consumer industry, consumer electronic devices have progressively become indispensable components of the constantly rising IoT. However, the steady rise of consumer IoT intelligent terminals has led to large-scale connections, spectrum scarcity, and energy consumption emerging as crucial challenges for the future wireless communication in resilient industry 5.0. To mitigate the aforementioned issues, a novel simultaneously transmitting and reflecting reconfigurable intelligent surface (STAR-RIS) assisted cognitive radio (CR)-non-orthogonal multiple access (NOMA) network are proposed. Specifically, we comprehensively elaborate on systems performance in terms of outage probability (OP), ergodic rate (ER) and energy efficiency (EE). Furthermore, the asymptotic OP and ER of the primary and secondary consumer electronic devices under the high signal-to-noise ratio (SNR) regions are investigated to undertake a thorough analysis. We find that the outage and ER performance gradually increase with the transmit SNR, and tend to a fixed value at high SNR regions. In addition, increasing the number of STAR-RIS components will enhance the reliable, ER and EE performance of the considered systems. Finally, the accuracy of analysis and the superiority of the proposed scheme are verified through Monte Carlo simulations.

*Index Terms*—Cognitive radio (CR), non-orthogonal multiple access (NOMA), resilient industry 5.0, simultaneously transmitting and reflecting reconfigurable intelligent surface (STAR-RIS).

## I. INTRODUCTION

The persistent prosperity of the Internet of Things (IoT) in resilient industry 5.0 is being driven by the development of the upcoming sixth generation (6G) wireless communication. As an emerging industry of the IoT, consumer electronic devices have played a pivotal role in advancing and popularizing intelligent terminals for consumers. The applications have expanded to various fields such as smart home, smart wearables, smart education, smart factory [1, 2]. In resilient industry 5.0, the pervasive utilization of consumer IoT intelligent terminals has resulted in large scale connectivity, high cost hardware, and energy consumption issues. To this end, several promising techniques are proposed, such as simultaneously transmitting and reflecting reconfigurable intelligent surface (STAR-RIS) [3], non-orthogonal multiple access (NOMA) [4] and cognitive radio (CR) [5].

Reconfigurable intelligent surface (RIS) has triggered an upsurge in research because of the ability to configure smart radio environments. RIS is a metasurface comprising plenty of inexpensive reflective elements that dynamically adjust the amplitude and phase of the reflective elements to achieve the desired path effect [6, 7]. However, the conventional RIS requires the transmitter and receiver being located on the same side, which inevitably creates blind spots behind the RIS, severely restricting its deployment flexibility and coverage range. In order to surmount this drawback, STAR-RIS was proposed in [8]. Unlike RIS, STAR-RIS has the capable to cover the entire space, achieving $360°$ full coverage [9]. Time switching, energy splitting and mode switching are the three representative protocols for STAR-RIS [10]. In [11], the authors modeled a STAR-RIS-NOMA network and explored its bit error performance under the imperfect successive interference cancellation (SIC) condition. To achieve maximum energy efficiency, Wang *et al.* in [12] alternately optimized the phase shift and beamforming vectors of the multi-user STAR-RIS-NOMA networks. In [13], the authors integrated cooperative dual RIS with STAR-RIS for the sake of communication in massive multiple input multiple output (MIMO) configurations.

The unprecedented prosperity of the consumer IoT within resilient industry 5.0 has resulted in a persistent escalation in the quantity of terminal connections. Fortunately, NOMA is propositioned as a potential candidate scheme for 6G due to the ability to achieve large scale connections [14]. NOMA, unlike traditional orthogonal multiple access (OMA), permits numerous users to access the same resource block at once, such as time/frequency/code domain resources [15]. It can significantly improve the resource utilization of communica-

Xingwang Li and Xuesong Gao are with the School of Physics and Electronic Information Engineering, Henan Polytechnic University, Jiaozuo, China (email: lixingwangbupt@gmail.com, gaoxuesong@home.hpu.edu.cn).

Liang Yang is with the College of Computer Science and Electronic Engineering, Hunan University, Changsha 410082, China (email: liangy@hnu.edu.cn).

Hongwu Liu is with the School of Information Science and Electrical Engineering, Shandong Jiaotong University, Jinan 250357, China (e-mail: liuhongwu@sdjtu.edu.cn).

Ji Wang is with the Department of Electronics and Information Engineering Central China Normal University, Wuha 430079, China (e-mail: jiwang@ccnu.edu.cn).

Khaled M. Rabie is with the Department of Engineering, Manchester Metropolitan University, M15 6BH Manchester, U.K. (e-mail: k.rabie@mmu.ac.uk).

Dawei Qiao is with the School of Emergency Management, Henan Polytechnic University, Jiaozuo, China (email: daweihpu@163.com.)

tion systems. At the transmitter, different transmit power is allocated according to the channel strength to achieve fairness among users, and signal separation is achieved at the receiver by means of the SIC technique [16]. To assess the performance of the system under consideration, Xu *et al.* in [17] provided a full-duplex network-coded cooperative NOMA model and derived the outage probability (OP) expressions. Zhang *et al.* in [18] introduced a novel low complexity scheme for the NOMA-unmanned aerial vehicle (UAV) networks in order to maximize the sum rate. Ding *et al.* in [19] offered a universal hybrid NOMA assisted mobile edge computing offloading scheme and established a multi-objective optimization issue with the objective of reducing energy consumption. To improve energy efficiency (EE), the authors in [20] combined incremental relaying with near user in the considered NOMA network, achieving an increase in throughput for far user.

In parallel, CR has been extensively investigated as a favorable technique to address the problem of spectrum resource scarcity [21]. The three typical modes of spectrum sharing in CR are interweave, overlay and underlay [22]. The CR network is split into the primary network (PN) with authorized primary users (PU) and the secondary network (SN) with unauthorized secondary users (SU). In CR network, SU can utilize the authorized frequency band of the PU and share spectrum resources with PU without affecting the quality of service (QoS) of the PU [23]. In overlay CR, the SN uses part of energy to transmit its own signals, while the remainder is used to help the PN transmit signals in exchange for the utilization of authorized frequency bands [24]. This mode enables synchronous transmission between the primary and secondary networks, while concurrently enhancing the performance of the PN. In [25], the authors presented an overlay CR-NOMA system and comprehensively assessed the reliability by calculating the expression of OP for primary and secondary users. To maximize average effective spectrum efficiency, Lu *et al.* in [26] proposed an optimization for a short packet covert communication in interweave CR. Further, the authors in [27] suggested a distributed transmit power control scheme for an underlay CR system to maximize spectrum efficiency.

In consideration of the aforementioned analysis, the combination of STAR-RIS, NOMA, and CR can achieve 360° full space coverage, which effectively improves spectrum utilization and communication QoS while achieving low power consumption. In [28], the authors proposed a coordinated direct and relay transmission based underlay CR-NOMA network, and the OP and throughput of users under imperfect SIC condition were investigated. Furthermore, the authors in [29] designed a hybrid transmission protocol and a user selection scheme for the multi-user underlay NOMA network. The authors in [30] optimized the system throughput for an UAV-assisted cooperative CR-NOMA network to attain the best performance under the imperfect SIC condition. In addition, the authors in [31] provided a general analysis framework in order to assess the coverage probability and ER of the STAR-RIS-NOMA networks. To reduce the average number of the lost data packets, the authors in [32] devised a new algorithm for the uplink energy harvesting-CR-NOMA networks. Li *et*

*al.* in [3] modeled a STAR-RIS assisted NOMA network with an illegal eavesdropper under the residual hardware impairments conditions. Further, with the aim of solving the secure communication problem brought on by the presence of eavesdroppers, the authors in [33] devised a secure communication strategy for the STAR-RIS-NOMA networks to maximize the secrecy rate.

### A. Motivation and Contributions

The development of consumer IoT is in full bloom, which has penetrated into various fields of life, such as smart homes, healthcare, intelligent transportation, environmental monitoring, etc. The major objective of this paper is to assist future consumer IoT networks achieve spectrum and massive connectivity in resilient industry 5.0. Although there is a significant amount of literature available on STAR-RIS, CR and NOMA, the integration of the three techniques is still in its infancy. In [34], the authors presented a novel beamforming design scheme for the RIS-aided in band full-duplex consumer IoT networks. However, NOMA, STAR-RIS and CR were not taken into account. The authors in [35] introduced a NOMA-enabled backscatter network in automotive industry 5.0 and designed a framework to maximize the EE. The downside is that there is no mention of STAR-RIS and CR technologies. To maximize the EE, Fang *et al.* in [36] designed an algorithm for the STAR-RIS-MIMO-NOMA systems. However, it should be noted that the above literature did not take into account the potential benefits of utilizing CR technology. Guo *et al.* in [37] investigated a STAR-RIS empowered non-terrestrial vehicle network with NOMA and evaluate the outage performance of all secondary vehicles. To tackle the critical security challenges faced by communication, the authors in [38] developed an artificial intelligence-based framework for the underlay CR-NOMA networks to maximize the secrecy EE. Liang *et al.* in [39] proposed a RIS assisted CR-NOMA model aimed at maximizing the EE while ensuring the QoS for PUs. However, STAR-RIS was not taken into account.

Motivated by the numerous benefits offered by STAR-RIS, CR and NOMA, we present the novel STAR-RIS assisted overlay CR-NOMA based consumer IoT networks for resilient industry 5.0. To assess the performance of the proposed system, we derive the analytical expressions of the OP, ER and EE. The main contributions of this paper are given as follows:

- We investigate the performance of the passive STAR-RIS assisted overlay CR-NOMA based consumer IoT networks for resilient industry 5.0 under the Nakagami-$m$ fading channels. The secondary transmitter assists the primary network transmission for access to the licensed bands. Due to the long distance between the secondary transmitter and consumer IoT devices, STAR-RIS is introduced to assist in the transmission of their messages.
- We calculate the analytical expressions of OP for the primary and secondary devices. The asymptotic performance of the devices under high signal-to-noise ratios (SNR) regions and the diversity orders are discussed. Based on the derived expressions, the reliable performance and the
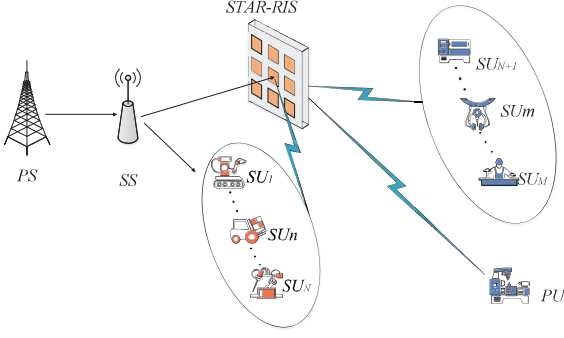
Fig. 1: The proposed system model in a resilient industry 5.0 environment

impact of the elements' number in STAR-RIS on the reliability of the considered system are assessed.

- The analytical expressions of ER for primary and secondary devices are deduced. The ER performance of the consumer electronic devices at high SNR regions is also investigated to gain insight into the STAR-RIS assisted CR-NOMA networks. In addition, the impact of the elements' numbers in STAR-RIS and the power allocation coefficients on the ER are analyzed.

- The EE for STAR-RIS assisted overlay CR-NOMA based consumer IoT networks in delay-tolerant transmission mode is analyzed. EE increase with the transmit SNR and the elements' number in STAR-RIS. Finally, we proved the superiority of the proposed networks through the Monte Carlo simulations.

### B. Organization and Notations

The remainder of this paper is structured as follows. Section II describes the STAR-RIS assisted overlay CR-NOMA based consumer IoT networks for resilient industry 5.0. Section III infers the analytical expressions of OP, the outage behavior of devices under high SNR regions and diversity order. Section IV explores the ER, the asymptotic ER under high SNR regions and EE. Section V confirms the correctness of the analysis through Monte Carlo simulation. Section VI summarizes the full paper.

The following are the meanings of the characters referenced in this paper. $E(x)$ represents the expectation of the random variable $x$, $diag(\cdot)$ is a diagonal matrix. $\mathcal{CN}(\mu, \sigma^2)$ denotes the complex Gaussian random variable with mean $\mu$ and variance $\sigma^2$. $\Gamma(\cdot)$ and $\gamma(\cdot)$ represent the gamma function and lower incomplete gamma function, respectively. $f_x(\cdot)$ and $F_x(\cdot)$ represent the probability density function (PDF) and the cumulative distribution function (CDF) of $x$.

## II. SYSTEM MODEL

Fig. 1 depicts a simultaneously transmitting and reflecting reconfigurable intelligent surface (STAR-RIS) assisted cognitive radio (CR)-non-orthogonal multiple access (NOMA) network in resilient industry 5.0, which comprises a primary station (PS), a secondary transmitter (SS), a STAR-RIS, $M$ secondary consumer Internet of Things (IoT) devices and a

primary consumer IoT device. It is assumed that there is no direct link between the PS and PU owing to severe fading or blockage [3], so the CR is introduced to assist the primary network in communication. Since SS is far away from devices, the STAR-RIS is installed to facilitate the transmission of messages between them. $SU_i, i \in \{1, \cdots, N\}$ is situated on the front side of the STAR-RIS, which can pick up signals from both SS and STAR-RIS reflections. $SU_i, i \in \{N+1, \cdots, M\}$ and PU are situated on the back side of STAR-RIS and can only receive the information transmitted by STAR-RIS. The channel coefficients for the links of PS-SS, SS-STAR-RIS, STAR-RIS-$SU_n$ ($1 \leq n \leq N$), SS-$SU_n$, STAR-RIS-$SU_m$ ($N+1 \leq m \leq M$), and STAR-RIS-PU can be represented as $h_{ss}$, $\mathbf{h}_{sr} \in \mathbb{C}^{1 \times L_r}$, $\mathbf{h}_{rn} \in \mathbb{C}^{L_r \times 1}$, $h_{sn}$, $\mathbf{h}_{rm} \in \mathbb{C}^{1 \times L_t}$, and $\mathbf{h}_{rp} \in \mathbb{C}^{L_t \times 1}$, respectively.

Without loss of generality, we presumptively believe that the channel gain from SS to $SU_i, i \in \{1, \cdots, N\}$ and from STAR-RIS to $SU_i, i \in \{N+1, \cdots, M\}$ is $|h_{su_1}|^2 \geq |h_{su_2}|^2 \geq \cdots |h_{su_N}|^2$ and $\left|h_{ru_{N+1}}\right|^2 \geq \left|h_{ru_{N+2}}\right|^2 \geq \cdots |h_{ru_M}|^2 \geq |h_{rp}|^2$, respectively. $\mathbf{\Phi}_T = diag\left(\sqrt{\beta_1^t}e^{j\theta_1^t}, ..., \sqrt{\beta_n^t}e^{j\theta_n^t}, ...\sqrt{\beta_N^t}e^{j\theta_N^t}\right)$ and $\mathbf{\Phi}_R = diag\left(\sqrt{\beta_1^r}e^{j\theta_1^r}, ..., \sqrt{\beta_n^r}e^{j\theta_n^r}, ...\sqrt{\beta_N^r}e^{j\theta_N^r}\right)$ are the transmitting and reflecting phase shifting matrices of the STAR-RIS, respectively. $\beta_n^t, \beta_n^r \in [0,1]$ and $\theta_n^r, \theta_n^t \in [0, 2\pi]$ represent the amplitude and phase shift of the $n$-th element of the STAR-RIS [1]. The following assumptions are considered: 1) both the PS, SS and the consumer electronic devices are equipped with a single antenna; 2) the element number in STAR-RIS is $L$; 3) all channels are subject to Nakagami-$m$ fading channels, i.e., $h_{ss} \sim Nakagami(m_{ss}, 1)$, $h_{su_i} \sim Nakagami(m_{su_i}, 1)$, $h_{sr,n} \sim Nakagami(m_{sr}, 1)$, $h_{ru_i,n} \sim Nakagami(m_{ru}, 1)$.

To facilitate hardware deployment, STAR-RIS adopts mode switching and the $L$ elements are divided into two parts, one serving $SU_i, i \in \{1, \cdots, N\}$ and the other serving $SU_i, i \in \{N+1, \cdots, M\}$. $L_r$ elements of the STAR-RIS completely reflect messages on the reflection links, while the remaining $L_t$ elements transmit messages on the transmission link, $L_r + L_t = L$. According to the mode switching protocol in [40], we set the amplitude parameter to $\beta_k^t = 0$ and $\beta_n^r = 1$ when the $L_r$ elements in reflection mode, and vice versa. We have $\beta_n^t = 1$ and $\beta_n^r = 0$ when $L_t$ elements in transmission mode. STAR-RIS has full reflection and full transmission two modes in mode switching by adjusting the amplitude coefficient, which brings it the advantage of being simple to deploy.

The received message at SS from PS is given by

$$y_{ss} = h_{ps}\sqrt{d_{ps}^{-\alpha_{ps}}P_p}x_p + n_s, \tag{1}$$

where $P_p$ indicates the transmit power of the PS, $x_p$ refers to the normalized message of PU with $E\left(|x_p|^2\right) = 1$, $d_{ps}$ and $\alpha_{ps}$ show the distance and path loss exponent for the PS-SS link, and $n_s \sim \mathcal{CN}(0, N_0)$ represents the complex additive white Gaussian noise (AWGN).

---

[1]The discussion of STAR-RIS-CR-NOMA network in this paper is based on optimal conditions as in [16], and the performance of the system in the presence of non-optimal phase noise condition will be further studied in the future.

The SS sends the superposed message to the PU and secondary devices. $SU_i, i \in \{1, \cdots, N\}$ receives messages from SS and STAR-RIS reflections, which can be written as

$$y_{su_n} = \left(h_{sn}\sqrt{d_{sn}^{-\alpha_{sn}}} + \mathbf{h}_{sr}\mathbf{\Phi}_R\mathbf{h}_{rn}\sqrt{d_{sr}^{-\alpha_{sr}}}\sqrt{d_{rn}^{-\alpha_{rn}}}\right) \quad (2)$$
$$\times \left(\sqrt{a_1 P_s}x_p + \sqrt{a_2 P_s}\sum_{i=1}^{M}\sqrt{b_i}x_{s,i}\right) + n_n,$$

where $d_{sn}$, $d_{sr}$, $d_{rn}$ and $\alpha_{sn}$, $\alpha_{sr}$, $\alpha_{rn}$ denote the distances and path loss exponents for the links of SS-$SU_n$, SS-STAR-RIS and STAR-RIS-$SU_n$, respectively. $n_n$ denotes AWGN and it follows $n_n \sim \mathcal{CN}(0, N_0)$. $a_1$ and $a_2$ refer to the power allocation parameters for the primary and secondary message satisfying $a_1 > a_2, a_1 + a_2 = 1$. $x_{s,i}$ and $b_i$ denote the message and the power allocation parameters for the $i$-th secondary devices, subject to $\sum_{i=1}^{M} b_i = 1$, $b_1 < \cdots < b_n \cdots < b_N < b_{N+1} \cdots < b_m \cdots < b_M$.

The received messages at $SU_m$ from STAR-RIS can be written as

$$y_{su_m} = \mathbf{h}_{sr}\mathbf{\Phi}_T\mathbf{h}_{rm}\sqrt{d_{sr}^{-\alpha_{sr}}d_{rm}^{-\alpha_{rm}}} \quad (3)$$
$$\times \left(\sqrt{a_1 P_s}x_p + \sqrt{a_2 P_s}\sum_{i=1}^{M}\sqrt{b_i}x_{s,i}\right) + n_m.$$

The received message at $PU$ can be given by

$$y_{rp} = \mathbf{h}_{sr}\mathbf{\Phi}_T\mathbf{h}_{rp}\sqrt{d_{sr}^{-\alpha_{sr}}d_{rp}^{-\alpha_{rp}}} \quad (4)$$
$$\times \left(\sqrt{a_1 P_s}x_p + \sqrt{a_2 P_s}\sum_{i=1}^{M}\sqrt{b_i}x_{s,i}\right) + n_p,$$

where $d_{rm}$, $d_{rp}$ and $\alpha_{rm}$, $\alpha_{rp}$ denote the distances and path loss exponents for the links of STAR-RIS-$SU_m$ and STAR-RIS-PU, respectively. $n_m$ and $n_p$ denote AWGN with mean power $N_0$.

### A. Received signal-to-interference-plus-noise (SINR)

Based on the above analysis, the SINR for decoding $x_p$ at SS can be represented as

$$\gamma_{ss}^{x_p} = \frac{|h_{ss}|^2 d_{ss}^{-\alpha_{ss}} P_p}{N_0}. \quad (5)$$

The SINR of decoding $x_p$ at the PU can be expressed as

$$\gamma_{pu} = \frac{|\mathbf{h}_{sr}\mathbf{\Phi}_T\mathbf{h}_{rp}|^2 d_{sr}^{-\alpha_{sr}}d_{rp}^{-\alpha_{rp}}a_1 P_s}{|\mathbf{h}_{sr}\mathbf{\Phi}_T\mathbf{h}_{rp}|^2 d_{sr}^{-\alpha_{sr}}d_{rp}^{-\alpha_{rp}}a_2 \sum_{i=1}^{M} b_i P_s + N_0}. \quad (6)$$

The SINR for $SU_m$ to decode PU's message $x_p$, $SU_{j_1}$'s message $x_{j_1}$, $j_1 \geq m$ and its own message are respectively written as

$$\gamma_{su_m,p} = \frac{|\mathbf{h}_{sr}\mathbf{\Phi}_T\mathbf{h}_{rp}|^2 d_{sr}^{-\alpha_{sr}}d_{rp}^{-\alpha_{rp}}a_1 P_s}{|\mathbf{h}_{sr}\mathbf{\Phi}_T\mathbf{h}_{rp}|^2 d_{sr}^{-\alpha_{sr}}d_{rp}^{-\alpha_{rp}}a_2 \sum_{i=1}^{M} b_i P_s + N_0}, \quad (7)$$

$$\gamma_{su_m,j_1} = \frac{|\mathbf{h}_{sr}\mathbf{\Phi}_T\mathbf{h}_{rm}|^2 d_{sr}^{-\alpha_{sr}}d_{rm}^{-\alpha_{rm}}a_2 b_{j_1} P_s}{|\mathbf{h}_{sr}\mathbf{\Phi}_T\mathbf{h}_{rm}|^2 d_{sr}^{-\alpha_{sr}}d_{rm}^{-\alpha_{rm}} P_s \Delta_1 + N_0}, \quad (8)$$

$$\gamma_{su_m} = \frac{|\mathbf{h}_{sr}\mathbf{\Phi}_T\mathbf{h}_{rm}|^2 d_{sr}^{-\alpha_{sr}}d_{rm}^{-\alpha_{rm}}a_2 b_m P_s}{|\mathbf{h}_{sr}\mathbf{\Phi}_T\mathbf{h}_{rm}|^2 d_{sr}^{-\alpha_{sr}}d_{rm}^{-\alpha_{rm}} P_s \Delta_2 + N_0}, \quad (9)$$

where $\Delta_1 = \sum_{q=1}^{j_1-1} a_2 b_q$ and $\Delta_2 = \sum_{q=1}^{m-1} a_2 b_q$.

The SINR for $SU_n$ to decode PU's message $x_p$, $SU_{j_2}$'s message $x_{j_2}$, $n \leq j_2 \leq N$ and its own message be given by

$$\gamma_{su_n,p} = \frac{|h_{sn} + \mathbf{h}_{sr}\mathbf{\Phi}_R\mathbf{h}_{rn}|^2 d_{sn}^{-2\alpha_{sn}}a_1 P_s}{|h_{sn} + \mathbf{h}_{sr}\mathbf{\Phi}_R\mathbf{h}_{rn}|^2 d_{sn}^{-2\alpha_{sn}}a_2 \sum_{i=1}^{M} b_i P_s + N_0}, \quad (10)$$

$$\gamma_{su_n,j_2} = \frac{|h_{sn} + \mathbf{h}_{sr}\mathbf{\Phi}_R\mathbf{h}_{rn}|^2 d_{sn}^{-2\alpha_{sn}}a_2 b_{j_2} P_s}{|h_{sn} + \mathbf{h}_{sr}\mathbf{\Phi}_R\mathbf{h}_{rn}|^2 d_{sn}^{-2\alpha_{sn}} P_s \Delta_3 + N_0}, \quad (11)$$

$$\gamma_{su_n} = \frac{|h_{sn} + \mathbf{h}_{sr}\mathbf{\Phi}_R\mathbf{h}_{rn}|^2 d_{sn}^{-2\alpha_{sn}}a_2 b_n P_s}{|h_{sn} + \mathbf{h}_{sr}\mathbf{\Phi}_R\mathbf{h}_{rn}|^2 d_{sn}^{-2\alpha_{sn}} P_s \Delta_4 + N_0}, \quad (12)$$

where $\Delta_3 = \sum_{q=1}^{j_2-1} a_2 b_q$ and $\Delta_4 = \sum_{q=1}^{n-1} a_2 b_q$.

### B. Channel Statistics of $SU_m$

The channel statistic by the moment matching method is obtained for analyzing the outage behavior of $SU_m$.

**Lemma 1.** Let $Y = \sum_{l=1}^{L_t} |h_{sr}||h_{rm}|$, the distribution of Y can be approximated as $Y \sim \Gamma(K_Y, \theta_Y)$ and the analytical expression of the PDF for the cascaded channel Y can be written as [16]

$$f_Y(x) = \frac{1}{\theta_Y^{K_Y}\Gamma(K_Y)}x^{K_Y-1}e^{-\frac{x}{\theta_Y}}, \quad (13)$$

where $K_Y = \frac{L_t \mu_m^2}{1-\mu_m^2}$, $\theta_Y = \frac{1-\mu_m^2}{\mu_m}$ and $\mu_m = E[|h_{sr}||h_{rm}|] = \left(\frac{1}{m_{sr}m_{rm}}\right)^{\frac{1}{2}}\frac{\Gamma(m_{sr}+\frac{1}{2})\Gamma(m_{rm}+\frac{1}{2})}{\Gamma(m_{sr})\Gamma(m_{rm})}$.

The channel statistic of the PU is the same as $SU_m$.

### C. Channel Statistics of $SU_n$

The series form of Laguerre polynomials is adopted to acquire the channel statistic and the results will be applied to discuss the outage behavior for $SU_n$.

**Lemma 2.** Let $X = |h_{sr}||h_{rn}|$, the PDF for the cascaded channel X is given as

$$f_X(z) = \frac{z^{\frac{m_{sr}+m_{rn}}{2}-1}}{\Gamma(m_{sr})\Gamma(m_{rn})}K_{m_{rn}-m_{sr}}(2\sqrt{z}). \quad (14)$$

Let $S = \sum_{l=1}^{L_r} |h_{sr}||h_{rn}|$. Since it is quite difficult to acquire the PDF of $S$ from (14), we obtain the PDF of $S$ through the series form of Laguerre polynomials [41]

$$f_S(x) \approx \frac{x^{\varphi_n}}{\phi_n^{\varphi_n+1}\Gamma(\varphi_n+1)}e^{-\frac{x}{\phi_n}}, \quad (15)$$

where $\varphi_n = \frac{\mu_n^2 L_r}{V_n} - 1$, $V_n = 1 - \mu_n^2$, $\phi_n = \frac{V_n}{\mu_n}$ and $\mu_n = E[|h_{sr}||h_{rn}|] = \left(\frac{1}{m_{sr}m_{rn}}\right)^{\frac{1}{2}}\frac{\Gamma(m_{sr}+\frac{1}{2})\Gamma(m_{rn}+\frac{1}{2})}{\Gamma(m_{sr})\Gamma(m_{rn})}$.

### III. OUTAGE PROBABILITY ANALYSIS

The reliability of the STAR-RIS assisted overlay CR-NOMA based consumer IoT networks for resilient industry 5.0 are evaluated in this section. Specifically, the analytical

expressions for the outage probability (OP) and the asymptotic behavior of consumer electronic devices in high SNR regions are derived. To gain more insight into the network, the diversity orders are discussed.

### A. The Outage Probability of PU

The PU will not be in outage only when both the SS and PU decode the message $x_p$ successfully. Thus, the OP of the PU can be indicated as

$$P_{out}^{PU} = 1 - \Pr\left(\gamma_{ss}^{x_p} > \gamma_{th}^{x_p}, \gamma_{pu} > \gamma_{th}^{x_p}\right), \qquad (16)$$

where $\gamma_{th}^{x_p} = 2^{R_{th}^{x_p}} - 1$ is the target SNR and $R_{th}^{x_p}$ is the target rate of detecting the message $x_p$.

**Theorem 1.** For the STAR-RIS-CR-NOMA network, the OP of PU under the Nakagami-$m$ fading channels is given by

$$P_{out}^{PU} = 1 - \theta_0 \left(\frac{1}{\theta_p}\right)^{-K_p} \frac{1}{\Gamma(K_p)\theta_p^{K_p}} \Gamma\left(K_p, \frac{\sqrt{\theta_1}}{\theta_p}\right), \quad (17)$$

where $\theta_0 = e^{-A}\sum_{m=0}^{m_{ss}-1}\frac{A^m}{m!}$, $A = \frac{m_{ss}\gamma_{th}^{x_p}N_0}{\Omega_{ss}P_p d_{ss}^{-\alpha_{ss}}}$, $\theta_1 = \frac{\gamma_{th}^{x_p}N_0}{d_{sr}^{-\alpha_{sr}}d_{rp}^{-\alpha_{rp}}P_s\left(a_1 - \gamma_{th}^{x_p}a_2\right)}$.

**Proof:** Please see Appendix A. ∎

**Corollary 1.** To get a clear exploration of the reliable performance, the asymptotic OP under the high SNR regions for PU can be given by

$$P_{out,\infty}^{PU} = 1 - \theta_0 \left(\frac{1}{\theta_p}\right)^{-K_p} \frac{1}{\Gamma(K_p)\theta_p^{K_p}} \Gamma\left(K_p, \frac{\sqrt{\theta_1'}}{\theta_p}\right), \qquad (18)$$

where $\theta_1' = \frac{\gamma_{th}^{x_p}}{d_{sr}^{-\alpha_{sr}}d_{rp}^{-\alpha_{rp}}\left(a_1 - \gamma_{th}^{x_p}a_2\right)}$.

**Proof:** Bring the transmit SNR $\gamma = \frac{P_s}{N_0}$, $\gamma \to \infty$ to (17), we can obtain (18). ∎

### B. The Outage Probability of $SU_m$

The following conditions must be met by $SU_m$ in order to avoid outage behavior: 1) SS decodes the message $x_p$ successfully; 2) $SU_m$ decodes the message $x_p$ of the primary device successfully; 3) $SU_m$ successfully decodes the message $x_{j_1}$ of $SU_{j_1}$; 4) $SU_m$ decodes its own message successfully. Therefore, its OP is given as

$$P_{out}^m = 1 - \Pr\left(E_{ss,p}\right)\Pr\left(E_{sm,p} \cap E_{sm,1} \cap \cdots \cap E_{sm,n}\right), \qquad (19)$$

where $E_{ss,p} = \left\{\gamma_{ss}^{x_p} > \gamma_{th}^{x_p}\right\}$, $E_{sm,p} = \left\{\gamma_{su_m,p} > \gamma_{th}^{x_p}\right\}$ and $E_{sm,j_1} = \left\{\gamma_{su_m,j_1} > \gamma_{th}^{x_{j_1}}\right\}$. $E_{ss,p}$ and $E_{sm,p}$ denote that the SS and $SU_m$ decode the message $x_p$ of the PU successfully. $E_{sm,j_1}$ means that the $SU_m$ successfully decodes the message $x_{j_1}$ of the $SU_{j_1}$, while $\gamma_{th}^{x_{j_1}} = 2^{R_{th}^{x_{j_1}}} - 1$ represents the target SNR of detecting the message $x_{j_1}$.

**Theorem 2.** The analytic expression of the OP for $SU_m$ can

be given by

$$P_{out}^m = 1 - \theta_0 \left(\frac{1}{\theta_x}\right)^{-2K_x} \left(\frac{1}{\Gamma(K_x)\theta_x^{K_x}}\right)^2 \Gamma\left(K_x, \frac{\sqrt{\theta_2}}{\theta_x}\right) \qquad (20)$$

$$\times \Gamma\left(K_x, \frac{\sqrt{\theta_3^*}}{\theta_x}\right),$$

where $\theta_2 = \frac{\gamma_{th}^{x_p}N_0}{d_{sr}^{-\alpha_{sr}}d_{rm}^{-\alpha_{rm}}P_s\left(a_1 - \gamma_{th}^{x_p}a_2\right)}$, $\theta_3 = \frac{\gamma_{th}^{j_1}N_0}{d_{sr}^{-\alpha_{sr}}d_{rm}^{-\alpha_{rm}}P_s\left(a_2 b_{j_1} - \gamma_{th}^{j_1}\Delta_1\right)}$, $\theta_3^* = \max_{1 \le j_1 \le M}\theta_3$.

**Proof:** According to (13) and (19), (20) will be acquired. ∎

**Corollary 2.** The asymptotic expression of OP for $SU_m$ under high SNR regions can be represented as

$$P_{out,\infty}^m = 1 - \theta_0 \left(\frac{1}{\theta_x}\right)^{-2K_x} \left(\frac{1}{\Gamma(K_x)\theta_x^{K_x}}\right)^2 \Gamma\left(K_x, \frac{\sqrt{\theta_2'}}{\theta_x}\right) \qquad (21)$$

$$\times \Gamma\left(K_x, \frac{\sqrt{\theta_3^{*'}}}{\theta_x}\right),$$

where $\theta_2' = \frac{\gamma_{th}^{x_p}}{d_{sr}^{-\alpha_{sr}}d_{rm}^{-\alpha_{rm}}\left(a_1 - \gamma_{th}^{x_p}a_2\right)}$, $\theta_3' = \frac{\gamma_{th}^{j_1}}{d_{sr}^{-\alpha_{sr}}d_{rm}^{-\alpha_{rm}}\left(a_2 b_{j_1} - \gamma_{th}^{j_1}\Delta_1\right)}$ and $\theta_3^{*'} = \max_{1 \le j_1 \le M}\theta_3'$.

**Proof:** Bring $\gamma = \frac{P_s}{N_0}$, $\gamma \to \infty$ to (20), we can obtain (21). ∎

### C. The Outage Probability of $SU_n$

To avoid outage at $SU_n$, the following conditions need to be met: 1) SS can decode the message $x_p$ of the PU successfully ; 2) $SU_n$ decodes the message $x_p$ successfully; 3) $SU_n$ successfully decodes the message $x_{j_2}$ of the $SU_{j_2}$; 4) $SU_n$ successfully decodes its own message. Accordingly, the OP of $SU_n$ is given by

$$P_{out}^n = 1 - \Pr\left(E_{ss,p}\right)\Pr\left(E_{sn,p} \cap E_{sn,1} \cap \cdots \cap E_{sn,n}\right), \qquad (22)$$

where $E_{sn,p} = \left\{\gamma_{su_n,p} > \gamma_{th}^{x_p}\right\}$ and $E_{sn,j_1} = \left\{\gamma_{su_n,j_2} > \gamma_{th}^{x_{j_1}}\right\}$. $E_{sn,p}$ denotes the case when $SU_n$ decodes the message $x_p$ of the primary device successfully, while $E_{sn,j2}$ represents the case when $SU_n$ successfully decodes the message $x_{j_2}$ of the $SU_{j_2}$. Finally, $\gamma_{th}^{x_{j_2}} = 2^{R_{th}^{x_{j_2}}} - 1$ represents the target SNR of devices $SU_{j_2}$ for detecting the message $x_{j_2}$.

**Theorem 3.** The analytic expression of the OP for $SU_n$ under the Nakagami-$m$ fading channel can be represented as

$$P_{out}^n = 1 - \theta_0\left(1 - \Delta_5 \times \Delta_6 - \Delta_7 \times \Delta_8 \times \Delta_9\right) \qquad (23)$$
$$\times\left(1 - \Delta_5 \times \Delta_{10} - \Delta_{11} \times \Delta_{12} \times \Delta_{13}\right),$$

where $\Delta_5 = \frac{1}{\phi_n^{\varphi_n+1}\Gamma(\varphi_n+1)}\left(\frac{1}{\phi_n}\right)^{-\varphi_n-1}$, $\Delta_6 = \gamma\left(\varphi_n+1, \frac{\sqrt{\theta_4}}{\phi_n}\right)$, $\Delta_7 = e^{-\sqrt{\theta_4}}(m_{ss}-1)!$, $\Delta_8 = \sum_{k=0}^{m_{ss}-1}\sum_{n=0}^{k_1}\binom{k_1}{n}\frac{\left(\sqrt{\theta_4}\right)^{k_1-n}}{k_1!}\left(\frac{1}{\phi_n}-1\right)^{-(n+\varphi_n)-1}$, $\Delta_9 = \gamma\left(n+\varphi_n+1, \sqrt{\theta_4}\left(\frac{1}{\phi_n}-1\right)\right)$, $\Delta_{10} =$

$\gamma\left(\varphi_n+1, \frac{\sqrt{\theta_5^*}}{\phi_n}\right)$, $\Delta_{11} = e^{-\sqrt{\theta_5^*}}(m_{ss}-1)!$, $\Delta_{12} =$

$\sum_{k=0}^{m_{ss}-1}\sum_{n=0}^{k_1}\begin{pmatrix} k_1 \\ n \end{pmatrix}\frac{(\sqrt{\theta_5^*})^{k_1-n}}{k_1!}\left(\frac{1}{\phi_n}-1\right)^{-(n+\varphi_n)-1}$,

$\Delta_{13} = \gamma\left(n+\varphi_n+1, \sqrt{\theta_5^*}\left(\frac{1}{\phi_n}-1\right)\right)$, $\theta_4 =$

$\frac{\gamma_{th}^{xp}N_0}{d_{sn}^{-2\alpha_{sn}}P_s\left(a_1-\gamma_{th}^{xp}a_2\sum_{i=1}^{M}b_i\right)}$, $\theta_5 = \frac{\gamma_{th}^{j_2}N_0}{d_{sn}^{-2\alpha_{sn}}P_s\left(a_2b_{j_2}-\Delta_3\right)}$ and

$\theta_5^* = \max\limits_{N+1\leq j_2\leq M}\theta_5$.

**Proof:** Please see Appendix B. ∎

**Corollary 3.** At high SNR regions, the asymptotic expression of OP for $SU_n$ can be represented as

$$P_{out,\infty}^n = 1-\theta_0\left(1-\Delta_{13}\times\Delta_{14}'-\Delta_{15}'\times\Delta_{16}'\times\Delta_{17}'\right) \quad (24)$$

$$\times\left(1-\Delta_5\times\Delta_{10}'-\Delta_{11}'\times\Delta_{12}'\times\Delta_{13}'\right),$$

where $\Delta_6' = \gamma\left(\varphi_n+1, \frac{\sqrt{\theta_4'}}{\phi_n}\right)$,

$\Delta_7' = e^{-\sqrt{\theta_4'}}(m_{ss}-1)!$, $\Delta_8' =$

$\sum_{k=0}^{m_{ss}-1}\sum_{n=0}^{k_1}\begin{pmatrix} k_1 \\ n \end{pmatrix}\frac{(\sqrt{\theta_4'})^{k_1-n}}{k_1!}\left(\frac{1}{\phi_n}-1\right)^{-(n+\varphi_n)-1}$,

$\Delta_9' = \gamma\left(n+\varphi_n+1, \sqrt{\theta_4'}\left(\frac{1}{\phi_n}-1\right)\right)$, $\Delta_{10}' =$

$\gamma\left(\varphi_n+1, \frac{\sqrt{\theta_5^{*\prime}}}{\phi_n}\right)$, $\Delta_{11}' = e^{-\sqrt{\theta_5^{*\prime}}}(m_{ss}-1)!$, $\Delta_{12}' =$

$\sum_{k=0}^{m_{ss}-1}\sum_{n=0}^{k_1}\begin{pmatrix} k_1 \\ n \end{pmatrix}\frac{(\sqrt{\theta_5^{*\prime}})^{k_1-n}}{k_1!}\left(\frac{1}{\phi_n}-1\right)^{-(n+\varphi_n)-1}$,

$\Delta_{13}' = \gamma\left(n+\varphi_n+1, \sqrt{\theta_5^{*\prime}}\left(\frac{1}{\phi_n}-1\right)\right)$, $\theta_4' =$

$\frac{\gamma_{th}^{xp}}{d_{sn}^{-2\alpha_{sn}}\left(a_1-\gamma_{th}^{xp}a_2\sum_{i=1}^{M}b_i\right)}$, $\theta_5' = \frac{\gamma_{th}^{j_2}}{d_{sn}^{-2\alpha_{sn}}\left(a_2b_{j_2}-\gamma_{th}^{j_2}\Delta_3\right)}$ and

$\theta_5^{*\prime} = \max\limits_{1\leq j_2\leq M}\theta_5'$.

**Proof:** Bring $\gamma=\frac{P_s}{N_0}$, $\gamma\to\infty$ to (23), we can obtain (24). ∎

### D. Diversity Order

We investigate the diversity orders for the consumer electronic devices to further understand the STAR-RIS assisted CR-NOMA systems. The following is the definition of the diversity order:

$$d = -\lim_{\gamma\to\infty}\frac{\log(P_{out}^\infty)}{\log\gamma}, \quad (25)$$

where $\gamma=\frac{P_s}{N_0}$.

**Corollary 4.** The diversity orders of PU, $SU_m$, $SU_{j_1}$, $SU_n$ and $SU_{j_2}$ can be represented as

$$d_{PU} = d_{SU_m} = d_{SU_{j_1}} = d_{SU_n} = d_{SU_{j_2}} = 0. \quad (26)$$

**Proof:** According to (18), (21) and (24), the result of (26) can be acquired. ∎

**Remark 1.** *From **Corollaries 1-4**, and **Theorems 1-3**, it can be observed that the OP decreases with the transmit SNR, while the reliability of the STAR-RIS assisted CR-NOMA networks increases and finally approaching a constant at high SNR regions. This means there are error floors, which leads*

*to the diversity orders of 0. In addition, the reliability of the considered network for resilient industry 5.0 gradually increases with the elements' numbers of STAR-RIS.*

## IV. ERGODIC RATE ANALYSIS

In this section, the ergodic rate (ER) performance of the STAR-RIS assisted overlay CR-NOMA networks are explored. Specifically, we derive the analytical expressions of ER and the asymptotic ER for the devices at high SNR regions to acquire a more profound comprehension of the system.

### A. The Ergodic Rate of PU

Based on the previous analysis, the ER of PU can be derived as

$$R_{PU} = E\left[\log_2\left(1+\gamma_{pu}\right)\right]. \quad (27)$$

Unfortunately, it is extremely difficult to acquire the exact expression, so we look for approximate but exact values instead.

**Theorem 4.** The ER for $PU$ in the STAR-RIS assisted CR-NOMA networks is given by

$$R_{PU} = \frac{\left(N_t\left(1-\mu_{pu}^2\right)+\mu_{pu}^2\right)d_{sr}^{-a_{sr}}d_{rpu}^{-a_{rp}}\alpha_1 P_s}{\left(N_t\left(1-\mu_{pu}^2\right)+\mu_{pu}^2\right)d_{sr}^{-a_{sr}}d_{rpu}^{-a_{rp}}\alpha_2\sum_{i=1}^{M}b_i P_s+N_0}. \quad (28)$$

**Proof:** Please see Appendix C. ∎

**Corollary 5.** The asymptotic expression of ER for $PU$ at high SNR regions can be represented as

$$R_{PU,\infty} = \frac{\alpha_1}{\alpha_2\sum_{i=1}^{M}b_i}. \quad (29)$$

### B. The Ergodic Rate of $SU_m$

The analytical expression of the ER for $SU_m$ can be represented as

$$R_m = E\left[\log_2\left(1+\gamma_{su_m}\right)\right]. \quad (30)$$

Similarly, we apply Jensen's inequality to calculate the approximate value of the ER for the $SU_m$.

**Theorem 5.** For the STAR-RIS-CR-NOMA networks, the ER for $SU_m$ under the Nakagami-$m$ fading channels is given by

$$R_m = \frac{\left(L_t\left(1-\mu_m^2\right)+\mu_m^2\right)d_{sr}^{-a_{sr}}d_{rm}^{-a_{rm}}\alpha_2 b_m P_s}{\left(L_t\left(1-\mu_m^2\right)+\mu_m^2\right)d_{sr}^{-a_{sr}}d_{rm}^{-a_{rm}}P_s\Delta_2+N_0}. \quad (31)$$

**Corollary 6.** The asymptotic expression of ER for $SU_m$ at high SNR regions can be given by

$$R_{m,\infty} = \frac{\alpha_2 b_m}{\Delta_2}. \quad (32)$$

### C. The Ergodic Rate of $SU_n$

The ER for $SU_n$ can be written as

$$R_n = E\left[\log_2\left(1+\gamma_{su_n}\right)\right]. \quad (33)$$

**Theorem 6.** Under Nakagami-$m$ fading channel, the ER for the $SU_n$ is given by

$$R_n = \frac{K_z \theta_z d_{sn}^{-2\alpha_{sn}} a_2 b_n P_s}{K_z \theta_z d_{sn}^{-2\alpha_{sn}} P_s \Delta_4 + N_0},\qquad(34)$$

where $K_Z = \frac{\mu_Z^2}{\mu_Z^{(2)} - \mu_Z^2}$, $\theta_Z = \frac{\mu_Z^{(2)} - \mu_Z^2}{\mu_Z^2}$, $\mu_Z = \frac{\Gamma(m_{sn}+1)}{m_{sn}\Gamma(m_{sn})} + \frac{\Gamma(L_r K_S + 2)\theta_S^2}{\Gamma(L_r K_S)} + \frac{2\Gamma(m_{sn}+\frac{1}{2})\Gamma(L_r K_S + 1)\theta_S}{(m_{sn})^{\frac{1}{2}}\Gamma(m_{ssn})\Gamma(L_r K_S)}$, $\mu_Z^{(2)} = \frac{\Gamma(m_{sn}+2)}{m_{sn}^2 \Gamma(m_{sn})} + \frac{\Gamma(L_r K_S + 4)\theta_S^4}{\Gamma(L_r K_S)} + \frac{6\Gamma(m_{sn}+1)\Gamma(L_r K_S + 2)\theta_S^2}{m_{sn}\Gamma(m_{sn})\Gamma(L_r K_S)} + \frac{4\Gamma(m_{sn}+\frac{3}{2})\Gamma(L_r K_S + 1)\theta_S}{(m_{sn})^{\frac{3}{2}}\Gamma(m_{sn})\Gamma(L_r K_S)} + \frac{4\Gamma(m_{sn}+\frac{1}{2})\Gamma(L_r K_S + 3)\theta_S^3}{(m_{sn})^{\frac{1}{2}}\Gamma(m_{sn})\Gamma(L_r K_S)}$, $K_S = \frac{\mu_n^2}{\mu_n^{(2)} - \mu_n^2}$ and $\theta_S = \frac{\mu_n^{(2)} - \mu_n^2}{\mu_n^2}$.

**Proof:** Please see Appendix D. ∎

**Corollary 7.** The asymptotic ER for $SU_n$ at high SNR regions is written as

$$R_{n,\infty} = \frac{\alpha_2 b_n}{\Delta_4}.\qquad(35)$$

### D. Energy efficiency

Energy efficiency (EE) is one of the key metrics to evaluate the performance of wireless communication systems. Generally speaking, delay-limited and delay-tolerant are its two transmission modes. The delay-tolerant transmission mode can be defined as the sum data rate divided by the total power consumption [42]. The following is the definition expression:

$$\eta = \frac{\text{Total date rate}}{\text{Total energy consumption}}\ (\text{bit/Joule}),\qquad(36)$$

The expression for the EE of the proposed system is represented as

$$\eta = \frac{R_{total}}{P_p + P_s + P_{STAR-RIS} + P_c}.\qquad(37)$$

where $R_{total} = R_{PU} + R_m + R_n$, $P_{STAR-RIS}$ and $P_c$ represent the hardware static dissipated power at the STAR-RIS and the constant circuit power consumption, respectively. **Remark 2.** *From **Corollaries 5-7**, and **Theorems 4-6**, we can find that the ER increases with the $P_s$, and the ER performance of the STAR-RIS-CR-NOMA networks increases and finally approaching a constant in high SNR regions. In addition, the ER performance of the considered network keeps increasing with the element number of STAR-RIS.*

## V. NUMERICAL RESULTS

We confirm the accuracy of the calculation by means of $10^5$ Monte Carlo simulation experiments [3]. The corresponding simulation parameters are presented in Table I unless otherwise noted. We assume the same parameters in the NOMA and OMA scenarios to ensure the fairness of the comparison. In addition, we set $M = 4$, $n = 1$, $j_2 = 2$, $m = 3$ and $j_1 = 4$, $L_r = L_t = 10$ [43].

Fig. 2 plots the OP versus the transmit SNR for the consumer electronic devices. It can be observed that the OP decreases with the SNR and finally converges to a constant value. The results show that the reliability increases with SNR and achieves a saturation state at high SNR regions. It indicates
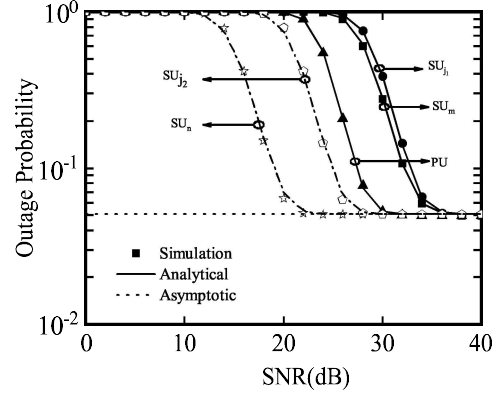


Fig. 2: The OP versus transmit SNR for different devices.
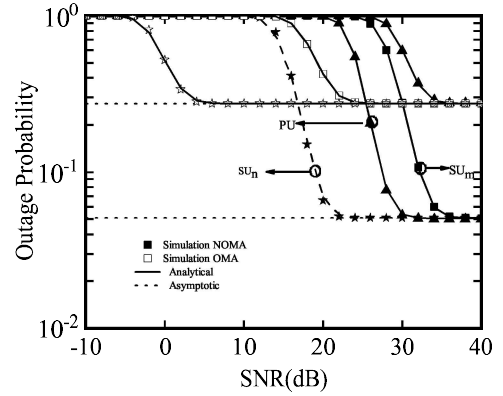


Fig. 3: The OP versus transmit SNR in NOMA and OMA conditions.

that continuing increasing the transmit SNR of the secondary devices after the saturation state will no longer be effective in enhancing the reliable performance of the STAR-RIS-CR-NOMA based consumer IoT networks in resilient industry 5.0. In addition, we find that the reflecting devices have superior reliable performance compared to the transmitting devices, which is due to the fact that there exists a direct link between SS and reflecting consumer electronic devices.

Fig. 3 depicts the OP of the devices in resilient industry 5.0 under NOMA and OMA scenarios. We assume that the parameters of the devices are the same in NOMA and OMA scenarios to ensure the fairness of the comparisons made. It is obvious to see that compared to OMA, PU has superior reliable performance in NOMA. The cause of this is that NOMA can enable numerous users to concurrently share the same wireless resources. For $SU_n$ and $SU_m$, NOMA performs better in high SNR regions, while its performance is worse in low SNR regions. This is because the SIC processes need to be executed to detect their own messages.

The impact of the STAR-RIS element number on system reliability is seen in Fig. 4. We set the target SNR as $\gamma_{th}^{x_p} = 0.001$, $\gamma_{th}^{x_m} = 0.001$, $\gamma_{th}^{x_{j2}} = 0.001$ and $L_t = L_r = L_\psi$. It is evident that when $N$ rises, the OP decreases, whereas the reliability of the network in resilient industry 5.0 gradually

**Table 1. TABLE OF PARAMETERS FOR NUMERICAL RESULTS [43]**

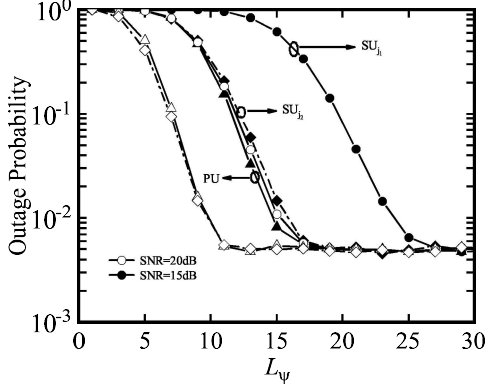| Channel fading parameters | $\{m_{ss}, m_{sr}, m_{rp}, m_{rm_{j1}}, m_{rm}, m_{sn_{j2}}, m_{sn}, m_{rn_{j2}}, m_{rn}\} = \{1, 0.7, 9, 3, 2, 9, 3, 1.8, 1.7\}$ |
|---|---|
| Power allocation coefficients | $\{a_1, a_2, b_{mj1}, b_m, b_{nj2}, b_n\} = \{0.6, 0.4, 0.4, 0.3, 0.2, 0.1\}$ |
| The distance parameters | $\{d_{ss}, d_{sr}, d_{rpu}, d_{rm_{j1}}, d_{rm}, d_{sn_{j2}}, d_{sn}, d_{rn_{j2}}, d_{rn}\} = \{10, 10, 100, 90, 80, 20, 10, 40, 10\}$ |
| Path loss exponents | $a = 2$ |
| Target rate | $\{R_{th}^{x_p}, R_{th}^{x_{j1}}, R_{th}^{x_m}, R_{th}^{x_{j2}}, R_{th}^{x_n}\} = \{0.015, 0.0015, 0.015, 0.015, 0.0015\}$ |



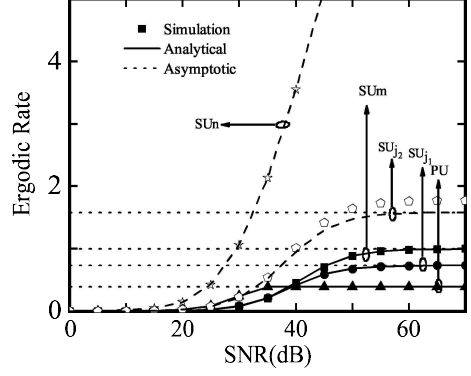Fig. 4: The OP versus the elements number in STAR-RIS



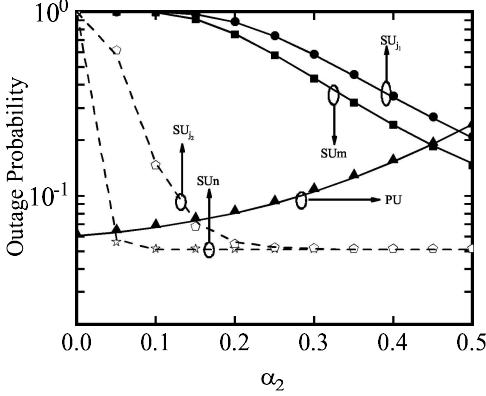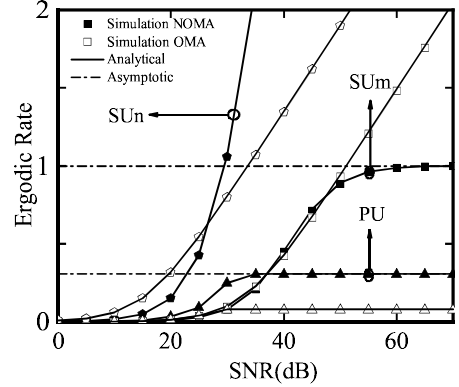Fig. 6: The ER versus the transmit SNR for different devices



Fig. 5: The OP versus the $a_2$ for different devices



Fig. 7: The ER versus transmit SNR under NOMA and OMA conditions

increases. Eventually, the OP converges to a fixed value at high SNR regions. The explanation is that the larger amount of elements in STAR-RIS, can yield better control of the communication links. However, increasing the elements number is no longer effective for the reliability of the STAR-RIS-CR-NOMA networks after the performance is saturated.

The effect of power allocation coefficient $a_2$ on OP for the consumer electronic devices is shown in Fig. 5. It can be found that as the $a_2$ increases, the OPs of SUs decrease, while the OPs of PU increase. This is due to the fact that when $a_2$ grows greater, the less power is allocated to the PU and the more likely an outage is to occur, and vice versa. In addition, the probability of outage in reflective devices are lower than that for transmit devices, as there is a direct connection channel between reflective devices and SS.

Fig. 6 depicts the relationship between ER and the transmit SNR for the devices. The parameters are set-

ting as $\{m_{ss}, m_{sr}, m_{rp}, m_{rm_{j1}}, m_{sn_{j2}}, m_{sn}, m_{rn_{j2}}, m_{rn}\} = \{5, 3, 8, 6, 6, 5, 5\}$, $\{a_{ss}, a_{sr}, a_{rp}, a_{rm_{j1}}, a_{rm}, a_{rn}, a_{rn_{j1}}\} = 1.8$, $\{a_{sn}, a_{sn_{j2}}\} = 3.6$. Noticeable from Fig. 6, the ERs of the devices increase with the transmit power $P_s$ and eventually converge to be constant. However, the ER of $SU_n$ increases with the SNR . This is due to the presence of the perfect SIC, which allows $SU_n$ to decode its own message without interference.

Fig. 7 shows the ERs of devices in resilient industry 5.0 under NOMA and OMA scenarios. It can be plainly viewed that the ER of PU is higher in NOMA scenario. The reason is that NOMA enables plenty users to concurrently share the same wireless resources. In the high SNR regions, $SU_n$ and $SU_m$ have better ERs in OMA scenario. The cause is that they need to perform SIC operations when decoding their own messages in NOMA network, while in OMA network, there
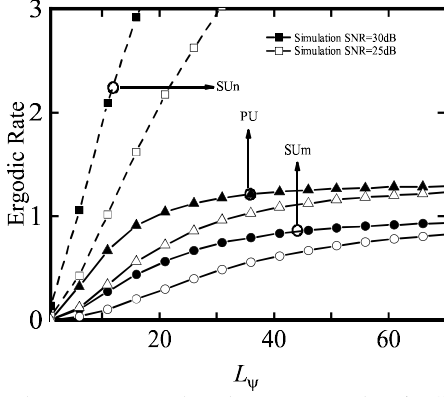
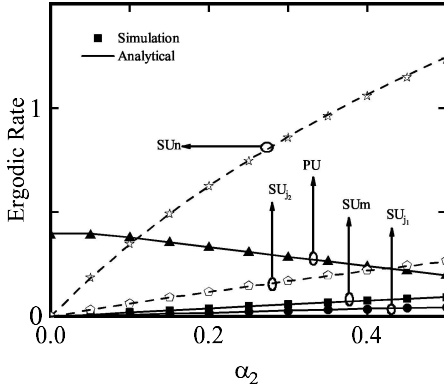Fig. 8: The ER versus the elements number in STAR-RIS



Fig. 9: The ER versus $a_2$ for different devices



(a) The OP versus $d_{rm}$ for $SU_m$

(b) The OP versus $d_{rpu}$ for $PU$

(c) The OP versus $d_{rn}$ for $SU_n$

(d) The ER versus $d_{rm}$ for $SU_m$

(e) The ER versus $d_{rpu}$ for $PU$

(f) The ER versus $d_{rn}$ for $SU_n$

Fig. 10: The OP and ER versus the distance

is no interference when decoding their own messages.

Fig. 8 plots the relationship of the ER and the number of STAR-RIS elements for the STAR-RIS assisted CR-NOMA networks at different transmit SNRs. We set the $\{m_{ss}, m_{sr}, m_{rp}, m_{rm_{j1}}, m_{sn_{j2}}, m_{sn}, m_{rn_{j2}}, m_{rn}\} = \{5, 3, 8, 6, 6, 5, 5\}$, $\{a_{ss}, a_{sr}, a_{rp}, a_{rm_{j1}}, a_{rm}, a_{rn}, a_{rn_{j1}}\} = 1.6$, $\{a_{sn}, a_{sn_{j2}}\} = 3.2$. As we can observe from Fig. 8, the ERs of devices increase with the elements number of STAR-RIS. It is attributed to the truth that the effectiveness of STAR-RIS in controlling communication links increases with the element number. The ER of $SU_n$ is more sensitive than $SU_m$. This is because the received messages at $SU_n$ is not only coming from SS, but also from the reflection of STAR-RIS. In addition, we find that the ERs of devices increase with the transmit SNR when the elements number of STAR-RIS is constant.

Fig. 9 plots the impact of $a_2$ on ER for the consumer electronic devices. We can observe that the theoretical analysis is in good match with the simulation results, which demonstrates the correctness of our study. It is shown that the ER of SUs consistently increases and the ER of PU keeps decrease with $a_2$. This is because the larger $a_2$, the greater the power allocated to SUs, so its ER continues to increase. This result can be obtained from (28), (31), (34).

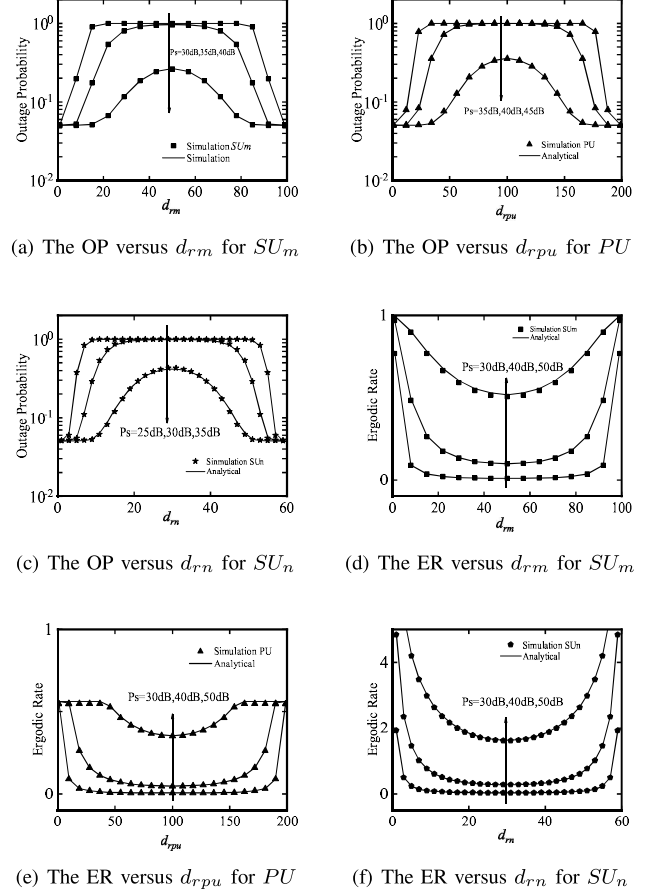Fig. 10 depicts the OP and ER versus the distance $d$ for the different consumer electronic devices in resilient industry 5.0. We can see that the OPs of the devices increase with distance and then start to decrease after reaching a certain value. $d$ has a worst value that maximises OP. The more it deviates from this worst value, the smaller the OP is and the more reliable the system will be. In addition, the ERs for devices tend to decrease and then increase with the distance. ER has a minimum value, and the farther the deviation distance is, the greater the ER will be. Furthermore, the OPs decrease and ERs increase with the transmit power $P_s$ when have a fixed distance.

Fig. 11 depicts the EE versus the transmit SNR under NOMA and OMA scenarios. We set $P_{STAR-RIS} = P_s = 5$ dB, $P_c = 0.1$ dB and $P_p = 10$ dB. It can be clearly observed that EE increases with the transmit SNR, and the system performance is better in NOMA scenario, which is due to the fact that NOMA allows multiple users to communicate simultaneously. In addition, EE increases as the number of elements in STAR-RIS. This indicates that the increase of the elements number in STAR-RIS has a positive impact on the system performance.

## VI. CONCLUSION

This paper presented a novel simultaneously transmitting and reflecting reconfigurable intelligent surface (STAR-RIS)
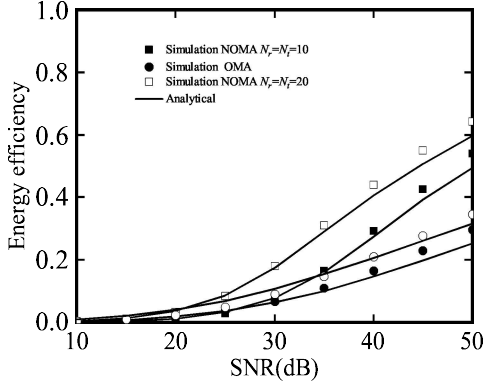
Fig. 11: The EE versus the transmit SNR

assisted overlay cognitive radio (CR)-non-orthogonal multiple access (NOMA) network based consumer Internet of Things (IoT) network in resilient industry 5.0. The performance of the network were explored by calculating the outage probabilities (OPs), ERs and energy efficiency (EE). Furthermore, the asymptotic expressions of OPs and ERs at high signal-to-noise ratio (SNR) regions were analyzed. On this basis, we investigated the diversity orders of devices. The correctness of our analysis results was confirmed by a number of simulation experiments. In addition, the influence of the number of STAR-RIS components, power allocation coefficient and the distance between STAR-RIS and devices on the system performance were discussed by simulation.

In addition, the performance can be further improved by optimize the number of STAR-RIS components, power allocation coefficient and the location of STAR-RIS. To make the scenario more practical, the impact of imperfect channel estimation information (CSI) and imperfect successive interference cancellation (SIC) on the system is also worthy of future research.

## APPENDIX A

By bringing (5), (6) into (16), the OP can be expressed as

$$
\begin{aligned}
P_{out}^{PU} &= 1 - \Pr\left(\gamma_{ss}^{x_p} > \gamma_{th}^{x_p}, \gamma_{pu} > \gamma_{th}^{x_p}\right) \\
&= 1 - \int_A^\infty f_{|h_{ps}|^2}(y)\,dy \int_B^\infty f_Y(x)\,dx \\
&= 1 - \theta_0\left(\frac{1}{\theta_p}\right)^{-K_p}\frac{1}{\Gamma(K_p)\theta_p^{K_p}}\Gamma\left(K_p, \frac{\sqrt{\theta_1}}{\theta_p}\right)
\end{aligned} \quad \text{(A.1)}
$$

where $A = \frac{\gamma_{th}^{x_p} N_0}{d_{ss}^{-a_{ss}} P_p}$ and $B = \frac{\gamma_{th}^{x_p} N_0}{d_{sr}^{-\alpha_{sr}} d_{rp}^{-\alpha_{rp}} P_s\left(a_1 - \gamma_{th}^{x_p} a_2 \sum_{i=1}^M b_i\right)}$.

The PDF of the channel $|h_{ss}|^2$ can be represented as

$$
f_{|h_{ss}|^2}(x) = \left(\frac{m_{ss}}{\Omega_{ss}}\right)^{m_{ss}}\frac{x^{m_{ss}-1}}{\Gamma(m_{ss})}e^{\left(-\frac{m_{ss}}{\Omega_{ss}}x\right)}, \quad \text{(A.2)}
$$

where $m_{ss}$ and $\Omega_{ss}$ refer to the Nakagami-$m$ fading severity parameter and the average power, respectively.

Bring (A.2) into (A.1) to obtain Eq. (17).

## APPENDIX B

The CDF of the channel $h_{sn}$ is given by

$$
F_{|h_{sn}|}(x) = 1 - \frac{\Gamma(m_{sn}, x)}{\Gamma(m_{sn})}. \quad \text{(B.1)}
$$

Assuming $Z = (|h_{sn}| + S)^2$, the expression of the PDF for Z can be expressed as

$$
F_Z(z) = \int_0^{\sqrt{z}} f_s(x) F_{|h_{sn}|}\left(\sqrt{z} - x\right) dx. \quad \text{(B.2)}
$$

According to (15), (B.1) and (B.2), the result of (23) can be obtained.

## APPENDIX C

The expression of ER for PU can be represented as

$$
R_{PU} = E\left[\log_2(1 + \gamma_{pu})\right] = \log_2\left(1 + E(\gamma_{pu})\right), \quad \text{(C.1)}
$$

According the $E\left[\log_2\left(1 + \frac{x}{y}\right)\right] = \log_2\left[1 + \frac{E(x)}{E(y)}\right]$, the expectation of the SINR $\gamma_{pu}$ can be written as

$$
E(\gamma_{pu}) = \frac{E\left(|\mathbf{h}_{sr}\mathbf{\Phi}_T\mathbf{h}_{rp}|^2\right)d_{sr}^{-\alpha_{sr}}d_{rp}^{-\alpha_{rp}}a_1 P_s}{E\left(|\mathbf{h}_{sr}\mathbf{\Phi}_T\mathbf{h}_{rp}|^2\right)d_{sr}^{-\alpha_{sr}}d_{rp}^{-\alpha_{rp}}a_2\sum_{i=1}^M b_i P_s + N_0}. \quad \text{(C.2)}
$$

Therefore, we only need to calculate the $E\left(|\mathbf{h}_{sr}\mathbf{\Phi}_T\mathbf{h}_{rp}|^2\right)$.

$$
E\left(|\mathbf{h}_{sr}\mathbf{\Phi}_T\mathbf{h}_{rp}|^2\right) = E(|\mathbf{h}_{sr}\mathbf{\Phi}_T\mathbf{h}_{rp}|)^2 + D\left(|\mathbf{h}_{sr}\mathbf{\Phi}_T\mathbf{h}_{rp}|\right), \quad \text{(C.3)}
$$

$$
\begin{aligned}
\mu_{pu} &= E\left[|h_{sr}||h_{rpu}|\right] \\
&= \left(\frac{1}{m_{sr}m_{rpu}}\right)^{\frac{1}{2}}\frac{\Gamma\left(m_{sr} + \frac{1}{2}\right)\Gamma\left(m_{rpu} + \frac{1}{2}\right)}{\Gamma(m_{sr})\Gamma(m_{rpu})}, \quad \text{(C.4)}
\end{aligned}
$$

$$
D(x) = N\left(1 - \mu_{pu}^2\right). \quad \text{(C.5)}
$$

Therefore, bringing (C.4) and (C.5) into (C.3) yields Eq. (26).

The calculation method of the $SU_m$ is similar to PU, so we omitted the calculation.

## APPENDIX D

The expression of ER for $SU_n$ can be represented as

$$
R_n = E\left[\log_2(1 + \gamma_{su_n})\right] = \log_2\left(1 + E(\gamma_{su_n})\right). \quad \text{(D.1)}
$$

As mentioned above, we directly calculate $E(\gamma_{su_n})$ as

$$
E(\gamma_{su_n}) = \frac{E\left(|h_{sn} + \mathbf{h}_{sr}\mathbf{\Phi}_R\mathbf{h}_{rn}|^2\right)d_{sn}^{-2a_{sn}}a_2 b_n P_s}{E\left(|h_{sn} + \mathbf{h}_{sr}\mathbf{\Phi}_R\mathbf{h}_{rn}|^2\right)d_{sn}^{-2a_{sn}}P_s\Delta_4 + N_0}. \quad \text{(D.2)}
$$

We set $Z = (S + h_{sn})^2$, it is approximated by the gamma distribution $Z \sim \Gamma(K_Z, \theta_Z)$.

The expectation of the Z can be represented as $E(Z) = K_Z\theta_Z$.

Bring the obtained $E(Z)$ to (D.2) to obtain Eq.(34).

## REFERENCES

[1] D. Pal, V. Vanijja, X. Zhang and H. Thapliyal, "Exploring the antecedents of consumer electronics IoT devices purchase decision: A mixed methods study," *IEEE Trans. Consum. Electron.*, vol. 67, no. 4, pp. 305-318, Nov. 2021.

[2] C. K. Wu, C. -T. Cheng, Y. Uwate, G. Chen, S. Mumtaz and K. F. Tsang, "State-of-the-art and research opportunities for next-generation consumer electronics," *IEEE Trans. Consum. Electron*, 2022.

[3] X. Li, Y. Zheng, M. Zeng, Y. Liu and O. A. Dobre, "Enhancing secrecy performance for STAR-RIS NOMA networks," *IEEE Trans. Veh. Technol.*, vol. 72, no. 2, pp. 2684-2688, Feb. 2023.

[4] X. Li, M. Liu, C. Deng, P. T. Mathiopoulos, Z. Ding and Y. Liu, "Full-Duplex Cooperative NOMA Relaying Systems With I/Q Imbalance and Imperfect SIC," *IEEE Wireless Commun. Lett.*, vol. 9, no. 1, pp. 17-20, Jan. 2020.

[5] A. Prathima, D. S. Gurjar, H. H. Nguyen and A. Bhardwaj, "Performance analysis and optimization of bidirectional overlay cognitive radio networks with hybrid-SWIPT," *IEEE Trans. Veh. Technol.*, vol. 69, no. 11, pp. 13467-13481, Nov. 2020.

[6] K. Guo and K. An, "On the performance of RIS-assisted integrated satellite-UAV-terrestrial networks with hardware impairments and interference," *IEEE Wireless Commun. Lett.*, vol. 11, no. 1, pp. 131-135, Jan. 2022.

[7] L. Yang, Y. Yang, D. B. d. Costa and I. Trigui, "Outage probability and capacity scaling law of multiple RIS-aided networks," *IEEE Wireless Commun. Lett.*, vol. 10, no. 2, pp. 256-260, Feb. 2021.

[8] J. Xu, Y. Liu, X. Mu, and O. A. Dobre, "STAR-RISs: simultaneous transmitting and reflecting reconfigurable intelligent surfaces, *IEEE Commun. Lett.*, vol. 25, no. 9, pp. 3134C3138, May 2021.

[9] Z. Zhang, Z. Wang, Y. Liu, B. He, L. Lv and J. Chen, "Security enhancement for coupled phase-shift STAR-RIS networks," *IEEE Trans. Veh. Technol.*, 2023.

[10] X. Mu, Y. Liu, L. Guo, J. Lin and R. Schober, "Simultaneously transmitting and reflecting (STAR) RIS aided wireless communications," *IEEE Trans. Wireless Commun.*, vol. 21, no. 5, pp. 3083-3098, May 2022.

[11] M. Aldababsa, A. Khaleel and E. Basar, "STAR-RIS-NOMA networks: An error performance perspective," *IEEE Commun. Lett.*, vol. 26, no. 8, pp. 1784-1788, Aug. 2022.

[12] T. Wang, F. Fang and Z. Ding, "Joint phase shift and beamforming design in a multi-user MISO STAR-RIS assisted downlink NOMA network," *IEEE Trans. Veh. Technol.*, 2023.

[13] A. Papazafeiropoulos, A. M. Elbir, P. Kourtessis, I. Krikidis and S. Chatzinotas, "Cooperative RIS and STAR-RIS assisted mMIMO communication: Analysis and optimization," *IEEE Trans. Veh. Technol.*, 2023.

[14] L. Yang et al., "Covert transmission and secrecy analysis of RS-RIS-NOMA-aided 6G wireless communication systems," *IEEE Trans. Veh. Technol.*, 2023.

[15] F. Kara and H. Kaya, "Error probability analysis of NOMA-based diamond relaying network," *IEEE Trans. Veh. Technol.*, vol. 69, no. 2, pp. 2280-2285, Feb. 2020.

[16] H. Liu, G. Li, X. Li, Y. Liu, G. Huang and Z. Ding, "Effective capacity analysis of STAR-RIS-assisted NOMA networks," *IEEE Wireless Commun. Lett.*, vol. 11, no. 9, pp. 1930-1934, Sep. 2022.

[17] B. Xu, Z. Xiang, P. Ren and X. Guo, "Outage performance of downlink full-duplex network-coded cooperative NOMA," *IEEE Wireless Commun. Lett.*, vol. 10, no. 1, pp. 26-29, Jan. 2021.

[18] R. Zhang, X. Pang, J. Tang, Y. Chen, N. Zhao and X. Wang, "Joint location and transmit power optimization for NOMA-UAV networks via updating decoding Order," *IEEE Wireless Commun. Lett.*, vol. 10, no. 1, pp. 136-140, Jan. 2021.

[19] Z. Ding, D. Xu, R. Schober and H. V. Poor, "Hybrid NOMA offloading in multi-user MEC networks," *IEEE Trans. Wireless Commun.*, vol. 21, no. 7, pp. 5377-5391, Jul. 2022.

[20] A. Jee and S. Prakriya, "Performance of Energy and Spectrally Efficient AF Relay-Aided Incremental CDRT NOMA Based IoT Network with Imperfect SIC for Smart Cities," *IEEE Internet Things J.*

[21] L. Li, H. Jiang and H. He, "Deep transfer cooperative sensing in cognitive radio," *IEEE Wireless Commun. Lett.*, vol. 10, no. 6, pp. 1354-1358, Jun. 2021.

[22] W. Xu, J. Zhang, P. Zhang and C. Tellambura, "Outage Probability of Decode-and-Forward Cognitive Relay in Presence of Primary User's Interference," *IEEE Commun. Lett.*, vol. 16, no. 8, pp. 1252-1255, Aug. 2012.

[23] D. Li, D. Zhang and J. Cheng, "A novel polarization enabled full-duplex hybrid spectrum sharing scheme for cognitive radios," *IEEE Commun. Lett.*, vol. 23, no. 3, pp. 530-533, Mar. 2019.

[24] Y. Zheng et al., "Overlay cognitive ABCom-NOMA-based ITS: An in-depth secrecy analysis," *IEEE Trans. Intell. Transp. Syst.*, vol. 24, no. 2, pp. 2217-2228, Feb. 2023.

[25] C. K. Singh and P. K. Upadhyay, "Overlay cognitive IoT-based full-duplex relaying NOMA systems with hardware imperfections," *IEEE Internet Things J.*, vol. 9, no. 9, pp. 6578-6596, May 2022.

[26] X. Lu, S. Yan, W. Yang, C. Liu and D. W. K. Ng, "Short-packet covert communication in interweave cognitive radio networks," *IEEE Trans. Veh. Technol.*, vol. 72, no. 2, pp. 2649-2654, Feb. 2023.

[27] W. Lee and K. Lee, "Deep learning-aided distributed transmit power control for underlay cognitive radio network," *IEEE Trans. Veh. Technol.*, vol. 70, no. 4, pp. 3990-3994, Apr. 2021.

[28] A. Jee, K. Agrawal, D. Johari and S. Prakriya, "Performance of CDRT-Based Underlay Downlink NOMA Network With Combining at the Users," *IEEE Trans. Cogn. Commun. Netw.*, vol. 9, no. 2, pp. 414-434, Apr. 2023.

[29] A. Jee, K. Janghel and S. Prakriya, "Performance of Adaptive Multi-User Underlay NOMA Transmission With Simple User Selection," *IEEE Trans. Cogn. Commun. Netw.*, vol. 8, no. 2, pp. 871-887, Jun. 2022.

[30] A. Bhowmick, S. D. Roy and S. Kundu, "Throughput maximization of a UAV assisted CR network with NOMA-based communication and energy-harvesting," *IEEE Trans. Veh. Technol.*, vol. 71, no. 1, pp. 362-374, Jan. 2022.

[31] Z. Xie, W. Yi, X. Wu, Y. Liu and A. Nallanathan, "STAR-RIS aided NOMA in multicell networks: A general analytical framework with gamma distributed channel modeling," *IEEE Trans. Commun.*, vol. 70, no. 8, pp. 5629-5644, Aug. 2022.

[32] Z. Shi, X. Xie, H. Lu, H. Yang, J. Cai and Z. Ding, "Deep reinforcement learning-based multidimensional resource management for energy harvesting cognitive NOMA communications," *IEEE Trans. Commun.*, vol. 70, no. 5, pp. 3110-3125, May 2022.

[33] Y. Han, N. Li, Y. Liu, T. Zhang and X. Tao, "Artificial noise aided secure NOMA communications in STAR-RIS networks," *IEEE Wireless Commun. Lett.*, vol. 11, no. 6, pp. 1191-1195, Jun. 2022.

[34] K. Singh, P. -C. Wang, S. Biswas, S. K. Singh, S. Mumtaz and C. -P. Li, "Joint Active and Passive Beamforming Design for RIS-Aided IBFD IoT Communications: QoS and Power Efficiency Considerations," *IEEE Trans. Consum. Electron.*, vol. 69, no. 2, pp. 170-182, May 2023.

[35] W. U. Khan, A. Ihsan, T. N. Nguyen, Z. Ali and M. A. Javed, "NOMA-Enabled Backscatter Communications for Green Transportation in Automotive-Industry 5.0," *IEEE Trans. Ind. Informat.*, vol. 18, no. 11, pp. 7862-7874, Nov. 2022.

[36] F. Fang, B. Wu, S. Fu, Z. Ding and X. Wang, "Energy-efficient design of STAR-RIS aided MIMO-NOMA networks," *IEEE Trans. Commun.*, vol. 71, no. 1, pp. 498-511, Jan. 2023.

[37] K. Guo, R. Liu, M. Alazab, R. H. Jhaveri, X. Li and M. Zhu, "STAR-RIS-empowered cognitive non-terrestrial vehicle network with NOMA," *IEEE Trans. Intell. Veh.*, 2023.

[38] C. E. Garcia, M. R. Camana and I. Koo, "Ensemble learning aided QPSOCbased framework for secrecy energy efficiency in FD CR-NOMA systems," *IEEE Trans. Green Commun. Netw.*, 2022.

[39] W. Liang, W. Luo, J. Zhang and Z. Ding, "Active and passive beamforming design for reconfigurable intelligent surface assisted CR-NOMA networks," *IEEE Commun. Lett.*, vol. 26, no. 10, pp. 2409-2414, Oct. 2022.

[40] Y. Liu et al., "STAR: Simultaneous transmission and reflection for 360° coverage by intelligent surfaces," *IEEE Wireless Commun.*, vol. 28, no. 6, pp. 102-109, Dec. 2021.

[41] S. Primak, V. Kontorovich, and V. Lyandres, *Stochastic Methods and their Applications to Communications: Stochastic Differential Equations Approach*, West Sussex, U.K. : Wiley, 2004.

[42] X. Li et al., "Cooperative Wireless-Powered NOMA Relaying for B5G IoT Networks With Hardware Impairments and Channel Estimation Errors," *IEEE Internet Things J.*, vol. 8, no. 7, pp. 5453-5467, Apr. 2021.

[43] X. Yue, J. Xie, Y. Liu, Z. Han, R. Liu and Z. Ding, "Simultaneously Transmitting and Reflecting Reconfigurable Intelligent Surface Assisted NOMA Networks," *IEEE Trans. Wireless Commun.*, vol. 22, no. 1, pp. 189-204, Jan. 2023.